Coupled reduced equations for strongly stratified flows

Cesar B. Rocha

June 30, 2016

Abstract

We present a set of reduced equations in the limit of strong stratification. The asymptotics lead to the hydrostatic primitive equations for the slow/large scale flow and non-hydrostatic, quasi-linear equations for the perturbations. There is no closure problem and the system conserves energy. We explore the properties of this coupled system of equations by studying solutions of a two-dimensional toy problem. This simple problem displays interesting dynamics with $\mathcal{O}(1)$ feedbacks between mean and perturbations. Even in this toy problem, the Reynolds stresses and buoyancy fluxes are not sign-definite in most of the regions of the parameter space.

1 Introduction

Strongly stratified turbulence has been used as a paradigm to interpret observations of strongly stratified turbulent geophysical flows [7]. Turbulence dominated by strong stable stratification occurs at scales larger than the Ozmidov scale, l_O,

$$l_O \stackrel{\text{def}}{=} \left(\frac{\epsilon}{N^3} \right)^{1/2} , \tag{1}$$

where ϵ is the kinetic energy rate of dissipation, and N is the buoyancy frequency. The Ozmidov scale is the horizontal scale of the largest overturns in a stratified flow. At scales much smaller than l_O, the flow is essentially unaffected by stratification, whereas at scales larger than l_O the effects of stratification dominates.

In the ocean l_O is $\mathcal{O}(1)$ m and in the atmosphere it is $\mathcal{O}(100)$ km [1, 3, 7]. At $\mathcal{O}(l_O)$ scales, the Rossby number of the flow is large and rotation is unimportant. The most prominent coherent structures that emerge in strongly stratified turbulence are strongly anisotropic. Indeed, stratified turbulence is often termed "pancake" turbulence [2, 7].

In the ocean, stratified turbulence is important at scales between 100 and 1 m and in the atmosphere at scales between 10 km and 100 m [7]. Kinetic and potential energy horizontal wavenumber spectra calculated from observations in the atmosphere and in the ocean are consistent with predictions of stably stratified turbulence[1]. These scales are barely resolved in regional models and not resolved at all in general circulation models. Understanding of the dynamics of strongly stratified turbulence, and in particular how the small scale stratified turbulence interacts with large scale flows, is important for parameterizing these effects into numerical models.

One approach towards understanding and modeling strongly stratified turbulence has been direct numerical simulations [1, 3, 7]. Figure 1 shows different regimes of

---

[1]The spectra are also consistent with predictions of other theories, e.g. [4].

stratified flows in the $\mathrm{Re} - 1/\mathrm{Fr}$ space, where (for details and definitions see section 2).

$$\mathrm{Fr} \overset{\text{def}}{=} \frac{\mathcal{U}}{N\mathcal{L}}, \qquad (2)$$

is the horizontal Froude number (and $1/\mathrm{Fr}^2$ is a measure of the strength of the stratification), and

$$\mathrm{Re} \overset{\text{def}}{=} \frac{\mathcal{U}\mathcal{L}}{\nu}, \qquad (3)$$

is the Reynolds number. Dimensional analysis suggests that strongly stratified turbulence regime develops when $\mathrm{ReFr}^2 > 1$ [3].
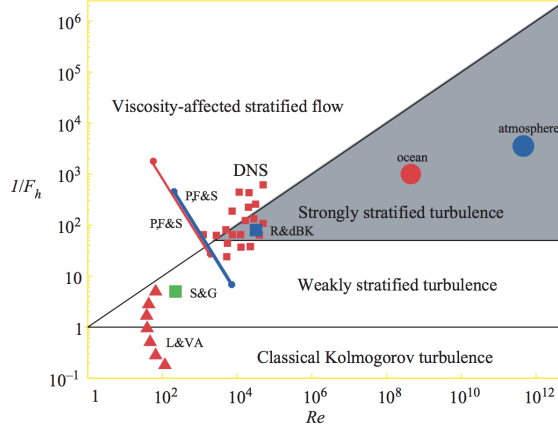

Figure 1: The different regimes of stratified flows as a function of the Reynolds number and the horizontal Froude number. Source: [3].

Direct numerical simulations with parameters of relevance to geophysical flows are currently unattainable through direct numerical simulations [1, 3]. Indeed, figure 1 shows that current direct numerical simulations are decades away in parameter space from the regimes of relevance to geophysical flows. Conclusions and extrapolations based on current low ReFr^2 simulations should be interpreted with care [1].

Here we take a different approach to study this problem. Inspired by the success of multi-scale asymptotics to study turbulent flows with strong constraints [6], e.g rotating convection [8], we dig deep into the scaling for strongly stratified flows and present a set of reduced equations for its modeling (Section 2). To explore the main properties of this system of equations and showcase its usefulness we study a toy initial value problem of stratified shear instability (Section 3). A summary and inquiries for future research are given in section 4.

2   Reduced equations for strongly stratified flows

Our starting point are the familiar Boussinesq equations. The momentum and mass conservation equations are reduced to

$$\partial_t \boldsymbol{u} + \boldsymbol{u} \cdot \boldsymbol{\nabla} \boldsymbol{u} = -\boldsymbol{\nabla} p + \nu \triangle \boldsymbol{u} - b\, \hat{\mathbf{k}}, \qquad (4)$$

and

$$\boldsymbol{\nabla} \cdot \boldsymbol{u} = 0, \qquad (5)$$

2

where $b \stackrel{\text{def}}{=} -\frac{g}{\rho_0}\rho$ is the negative of the reduced gravity, commonly referred to buoyancy in the oceanographic community (e.g., [9]), and $\hat{k}$ is the unit vector in the vertical direction. The system is closed with the thermodynamic equation

$$\partial_t b + \boldsymbol{u} \cdot \boldsymbol{\nabla} b = \kappa \triangle b - N^2(z)\, w\,, \tag{6}$$

where $N^2(z) = \frac{\partial B}{\partial z}$ is the background buoyancy frequency.

We start by nondimensionalizing the Boussinesq equations (4)-(6). Let

$$(x,y) = (x^\star, y^\star)\,\mathcal{L}\,, \qquad z = z^\star\,\mathcal{H}\,, \qquad (u,v) = (u^\star, v^\star)\,\mathcal{U}\,, \qquad t = t^\star\frac{\mathcal{L}}{\mathcal{U}}\,, \qquad p = p^\star\,\mathcal{U}^2\,. \tag{7}$$

From the vertical momentum equation we find the scale for the buoyancy is

$$b = b^\star\frac{\mathcal{U}^2}{\mathcal{H}}\,. \tag{8}$$

To find a scale for the vertical velocity, we insist that the horizontal advection of buoyancy balances, to lowest order, the vertical advection of background buoyancy in (6). Hence

$$w = w^\star\frac{\text{Fr}^2}{\alpha}\mathcal{U}\,, \tag{9}$$

where the horizontal Froude number is

$$\text{Fr} \stackrel{\text{def}}{=} \frac{\mathcal{U}}{N\mathcal{L}}\,, \tag{10}$$

and the aspect ratio of the flow is

$$\alpha \stackrel{\text{def}}{=} \frac{\mathcal{H}}{\mathcal{L}}\,. \tag{11}$$

Using the scaling (7) through (9) in the Boussinesq equations (4) through (6), we obtain

$$\partial_{t^\star}\boldsymbol{u}_h^\star + \boldsymbol{u}_h^\star \cdot \boldsymbol{\nabla}^\star\boldsymbol{u}_h^\star + \frac{\text{Fr}^2}{\alpha^2}w^\star\partial_{z^\star}\boldsymbol{u}_h^\star = -\boldsymbol{\nabla}_h^\star p^\star + \frac{1}{\text{Re}}\left[\triangle_h^\star\boldsymbol{u}_h^\star + \frac{1}{\alpha^2}\partial_{z^\star}^2\boldsymbol{u}_h^\star\right]\,, \tag{12}$$

$$\text{Fr}^2\left[\partial_{t^\star}w_h^\star + \boldsymbol{u}_h^\star \cdot \boldsymbol{\nabla}^\star w_h^\star + \frac{\text{Fr}^2}{\alpha^2}\partial_{z^\star}w^\star\right] = -\partial_{z^\star}p^\star + b^\star + \frac{\text{Fr}^2}{\text{Re}}\left[\triangle_h^\star w^\star + \frac{1}{\alpha^2}\partial_{z^\star}^2 w^\star\right]\,, \tag{13}$$

$$\boldsymbol{\nabla}^\star \cdot \boldsymbol{u}_h^\star + \frac{\text{Fr}^2}{\alpha^2}\partial_{z^\star}w^\star = 0\,, \tag{14}$$

and

$$\partial_{t^\star}b^\star + \boldsymbol{u}_h^\star \cdot \boldsymbol{\nabla}^\star b^\star + \frac{\text{Fr}^2}{\alpha^2}w^\star\partial_{z^\star}b^\star = w + \frac{1}{\text{Re}\,\text{Pr}}\left[\triangle_h^\star b^\star + \frac{1}{\alpha^2}\partial_{z^\star}^2 b^\star\right]\,, \tag{15}$$

where the Reynolds number is

$$\text{Re} \stackrel{\text{def}}{=} \frac{\mathcal{U}\mathcal{L}}{\nu}\,, \tag{16}$$

and the Prandtl number is

$$\text{Pr} \stackrel{\text{def}}{=} \frac{\kappa}{\nu}\,. \tag{17}$$

From now on, we drop the star super scripts — all variables are nondimensional unless otherwise stated.

Note that a full quasi-two-dimensionalization of the system (to lowest order in Fr) depends on the ratio $\frac{\text{Fr}^2}{\alpha^2}$ [2]. If that ratio goes to zero as Fr $\to 0$, then the system

3

consists of two-dimensional layers, with properties similar to two-dimensional turbulence. Alternatively, a more interesting case is when the aspect ratio α adjust so that $\frac{\text{Fr}}{\alpha} = \mathcal{O}(1)$ (see appendix A for details). This implies that the vertical scale of the motion is

$$\mathcal{H} \sim \frac{\mathcal{U}}{N}. \tag{18}$$

Notice that with this scaling, the potential energy of the flow has the same order of the kinetic energy

$$\frac{b^2}{N^2} = \frac{\text{Fr}^2}{\alpha^2}\mathcal{U}^2 \sim \mathcal{O}(\mathcal{U}^2), \tag{19}$$

and therefore there is an approximate equipartition between kinetic energy and potential energy.

We assume that the system evolves in two different sets of scales. That is, all fields depend on fast/short scales (χ_h, τ) and slow/long $(\mathbf{x}_h, t)$. A single vertical scale is assumed. The fast time variable is

$$\tau \stackrel{\text{def}}{=} \text{Fr}^{-1}\, t, \qquad \text{so that} \qquad \partial_t \to \partial_t + \text{Fr}^{-1}\partial_\tau. \tag{20}$$

Similarly, the horizontal short spatial variable is

$$\boldsymbol{\chi} \stackrel{\text{def}}{=} \text{Fr}^{-1}\, \boldsymbol{x}, \qquad \text{so that} \qquad \boldsymbol{\nabla}_h^{\boldsymbol{x}} \to \boldsymbol{\nabla}_h^{\boldsymbol{x}} + \text{Fr}^{-1}\boldsymbol{\nabla}_h^{\boldsymbol{\chi}}. \tag{21}$$

Any field f depends on both fast/short and slow/long scales, and is decomposed into

$$f = \bar{f} + \text{Fr}^n f' + o(\text{Fr}^n), \tag{22}$$

where the overbar denotes the average over the slow/short scales (e.g. [6]):

$$\bar{f}(\boldsymbol{x}, t, z) \stackrel{\text{def}}{=} \lim_{S,T \to \infty} \frac{1}{S\,T} \iint_{\mathcal{A}} \int_T f(\boldsymbol{x}, t, \tau, \boldsymbol{\chi}, z)\mathrm{d}\tau\mathrm{d}\vec{\chi}. \tag{23}$$

Note that, by definition, $\bar{f}' = 0$. The correct power n depends on the dynamical field, and is chosen in order to obtain a nontrivial balance. We have

$$\begin{aligned}
\boldsymbol{u}_h &= \bar{\boldsymbol{u}}_h + \text{Fr}^{1/2}\, \boldsymbol{u}_h' + \mathcal{O}(\text{Fr}^{3/2}), \\
p &= \bar{p} + \text{Fr}^{1/2}\, p' + \mathcal{O}(\text{Fr}^{3/2}), \\
b &= \bar{b} + \text{Fr}^{1/2}\, b' + \mathcal{O}(\text{Fr}^{3/2}), \\
w &= \bar{w} + \text{Fr}^{-1/2}\, w' + \mathcal{O}(\text{Fr}^0).
\end{aligned} \tag{24}$$

Note that, in dimensional form, the fluctuations are isotropic, i. e., $(\boldsymbol{u}_h', w') \sim \text{Fr}^{1/2}\mathcal{U}$.

Reduced equations for $\text{Fr} \ll 1$ and $\text{Re} \gg 1$

We now introduce the rescaled operators (20) and (21) into the nondimensional equations (12) through (15), and average over the fast/short scales to obtain

$$\partial_t \bar{\boldsymbol{u}}_h + \bar{\boldsymbol{u}}_h \cdot \boldsymbol{\nabla}_h^{\boldsymbol{x}}\bar{\boldsymbol{u}}_h + \bar{w}\partial_z\bar{\boldsymbol{u}}_h = -\boldsymbol{\nabla}_h^{\boldsymbol{x}}\bar{p} + \frac{1}{\text{Re}_b}\partial_z^2\bar{\boldsymbol{u}}_h - \partial_z(\overline{w'\boldsymbol{u}_h'}), \tag{25}$$

$$0 = -\partial_z\bar{p} + \bar{b}, \tag{26}$$

$$\boldsymbol{\nabla}_h^{\boldsymbol{x}} \cdot \bar{\boldsymbol{u}}_h + \partial_z\bar{w} = 0, \tag{27}$$

4

and

$$\partial_t \bar{b} + \bar{\boldsymbol{u}}_h \cdot \boldsymbol{\nabla}_h^{\boldsymbol{x}} \bar{b} + \bar{w}\partial_z \bar{b} = -\bar{w} + \frac{1}{\mathrm{Re}_b \,\mathrm{Pr}}\partial_z^2 \bar{b} - \partial_z(\overline{w'b'})\,, \tag{28}$$

where the buoyancy Reynold number is $\mathrm{Re}_b \stackrel{\text{def}}{=} \mathrm{Fr}^2 \,\mathrm{Re}$.

The equations for the perturbations are obtained by subtracting the mean equations above from Boussinesq equations (with $\mathrm{Fr} \ll 1$ and $\mathrm{Re} \gg 1$). We obtain, to lowest order,

$$\partial_\tau \boldsymbol{u}_h' + \bar{\boldsymbol{u}}_h \cdot \boldsymbol{\nabla}_h^\chi \boldsymbol{u}_h' + w'\partial_z \bar{\boldsymbol{u}}_h = -\boldsymbol{\nabla}_h^\chi p' + \frac{\mathrm{Fr}}{\mathrm{Re}_b}\left(\triangle_h^\chi + \partial_z^2\right)\boldsymbol{u}_h'\,, \tag{29}$$

$$\partial_\tau w' + \bar{\boldsymbol{u}}_h \cdot \boldsymbol{\nabla}_h^\chi w' = -\partial_z p' + b' + \frac{\mathrm{Fr}}{\mathrm{Re}_b}\left(\triangle_h^\chi + \partial_z^2\right)w'\,, \tag{30}$$

$$\partial_\tau b' + \bar{\boldsymbol{u}}_h \cdot \boldsymbol{\nabla}_h^\chi b' + w'(\partial_z \bar{b} + 1) = \frac{\mathrm{Fr}}{\mathrm{Re}_b \,\mathrm{Pr}}\left(\triangle_h^\chi + \partial_z^2\right)b'\,, \tag{31}$$

$$\boldsymbol{\nabla}_h^\chi \cdot \boldsymbol{u}_h' + \partial_z w' = 0\,. \tag{32}$$

In some calculations, it is convenient to rewrite the equations for the perturbations (29) through (32) in terms of the slow/small scale independent variables. For future reference, these equations are:

$$\mathrm{Fr}\left(\partial_t \boldsymbol{u}_h' + \bar{\boldsymbol{u}}_h \cdot \boldsymbol{\nabla}_h^{\boldsymbol{x}} \boldsymbol{u}_h'\right) + w'\partial_z \bar{\boldsymbol{u}}_h = -\mathrm{Fr}\boldsymbol{\nabla}_h^{\boldsymbol{x}} p' + \frac{\mathrm{Fr}}{\mathrm{Re}_b}\left(\mathrm{Fr}^2 \triangle_h^{\boldsymbol{x}} + \partial_z^2\right)\boldsymbol{u}_h'\,, \tag{33}$$

$$\mathrm{Fr}\left(\partial_t w' + \bar{\boldsymbol{u}}_h \cdot \boldsymbol{\nabla}_h^{\boldsymbol{x}} w'\right) = -\partial_z p' + b' + \frac{\mathrm{Fr}}{\mathrm{Re}_b}\left(\mathrm{Fr}^2 \,\triangle_h^{\boldsymbol{x}} + \partial_z^2\right)w'\,, \tag{34}$$

$$\mathrm{Fr}\left(\partial_t b' + \bar{\boldsymbol{u}}_h \cdot \boldsymbol{\nabla}_h^{\boldsymbol{x}} b'\right) + w'(\partial_z \bar{b} + 1) = \frac{\mathrm{Fr}}{\mathrm{Re}_b \,\mathrm{Pr}}\left(\mathrm{Fr}^2 \,\triangle_h^{\boldsymbol{x}} + \partial_z^2\right)b'\,, \tag{35}$$

$$\mathrm{Fr}\,\boldsymbol{\nabla}_h^{\boldsymbol{x}} \cdot \boldsymbol{u}_h' + \partial_z w' = 0\,. \tag{36}$$

Alternatively, the quasi-linear system above can be expressed in terms of a single variable w'

$$\left[\mathsf{L}^\chi - \frac{\mathrm{Fr}}{\mathrm{Re}_b \,\mathrm{Pr}}\left(\triangle_h^\chi + \partial_z^2\right)\right]\left[\mathsf{L}^\chi\left(\triangle_h^\chi + \partial_z^2\right) - \partial_z^2 \bar{\boldsymbol{u}}_h \cdot \boldsymbol{\nabla}_h^\chi\right]w' + (\partial_z \bar{b} + 1)\triangle_h^\chi w'$$

$$= \frac{\mathrm{Fr}}{\mathrm{Re}_b}\left[\mathsf{L}^\chi - \frac{\mathrm{Fr}}{\mathrm{Re}_b \,\mathrm{Pr}}\left(\triangle_h^\chi + \partial_z^2\right)\right]\left(\triangle_h^\chi + \partial_z^2\right)^2 w'\,, \tag{37}$$

where the quasi-linear operator is

$$\mathsf{L}^\chi \stackrel{\text{def}}{=} \partial_\tau + \bar{\boldsymbol{u}}_h \cdot \boldsymbol{\nabla}_h^\chi\,. \tag{38}$$

The two-dimensional (x, z) version of (37) reduces to the Taylor-Goldstein equation in the inviscid limit (see appendix B).

Conservation of energy

The coupled system (25)-(28) and (29)-(31) conserves total energy in the inviscid limit $(\mathrm{Re} \to \infty)$

$$\frac{\mathrm{d}E}{\mathrm{d}t} = 0\,, \tag{39}$$

where the nondimensional total energy is

$$E = \frac{1}{2}\iiint\left[\left(|\bar{\boldsymbol{u}}_h|^2 + \bar{b}^2\right) + \mathrm{Fr}\left(\overline{|\boldsymbol{u}_h'|^2} + \overline{w'^2} + \overline{b'^2}\right) + \mathcal{O}(\mathrm{Fr}^2)\right]\mathrm{d}V\,, \tag{40}$$

5

and we assumed harmless boundary conditions such as no-flux or triple periodicity (see appendix C for details). The dimensional potential energy has the form b^2/N^2. To lowest order the kinetic energy is due to the horizontal flow. Consistent with our approximation, the system is isotropic at $\mathcal{O}(\mathrm{Fr})$.

3 Decaying problems

To begin exploring the reduced system, we study solutions of a very simplified problem. We consider two-dimensional system $(x - z)$ with solutions of the slow field independent of the slow horizontal coordinate (x). In other words, the "pancakes" are infinitely long. A different interpretation is that we are looking for the zeroth mode of the slow field, or the x-average. Thus, the slow/long equations reduce to

$$\partial_t \bar{\boldsymbol{u}}_h = \frac{1}{\mathrm{Re}_b} \partial_z^2 \bar{\boldsymbol{u}}_h - \partial_z \overline{w' \boldsymbol{u}'_h}, \tag{41}$$

$$\partial_t \bar{b} = \frac{1}{\mathrm{Re}_b \, \mathrm{Pr}} \partial_z^2 \bar{b} - \partial_z \overline{w' b'}. \tag{42}$$

In the absence of perturbations, these equations simply reduce to the diffusion equation.

The initial conditions for this toy problem consists of two shear layers, with a strong stratification across the shear regions, and very low stratification between the layers. The two shear-layer set up was chosen for numerical convenience owing to its periodicity in z. The functional forms are

$$\bar{u}(z) = \tanh\left[m_0 \left(z - \tfrac{\pi}{2}\right)\right] - \tanh\left[m_0 \left(z - \tfrac{3\pi}{2}\right)\right] - 1, \tag{43}$$

and

$$\bar{b}(z) = A_0 \left(\tanh[m_0(z - \tfrac{3\pi}{2})] - \tanh[m_0(z - \tfrac{\pi}{2})]\right)\left(z - \pi\right). \tag{44}$$

Notice that the total background stratification is $B(z) = z + \bar{b}$. In the following experiments, we fix the mean shear m_0 and vary the distance between the two shear layers (Figure 2). We also fix Fr $= 0.02$ and Pr $= 1$.

The slow equations (41) and (42) together with the fast equations are solved (29) through (36) are sovled numerically with a standard Fourier spectral method. The whole system is solved in a single spatial scale and a single time scale. To compute the fluxes whose divergences force the slow equations, we only average the perturbations in space; solutions are not very sensitive to average both in space and time (see appendix D). The system is marched forward using a fourth order implicit-explicit Runge-Kutta time stepper.

3.1 Linear stability analysis

Using the stationary mean velocity (43) and stratification (44), we perform a linear stability analysis of the quasilinear equations for the perturbations. Figure 3 shows the growth rates for the base state profiles with $h = 1$ through $h = 1/8$ and various Re_b. The growth rates increase with Re_b. For large h, where the two shear layers are virtually independent the unstable modes span a wider region of the horizontal wavenumber space, whereas for small h the unstable modes are confined to wavenumbers $k < 10$. The growth rate of the most unstable mode increase with decreasing h. There is no dramatic transition of the stability properties as a function of Re_b, but the growth rates increase significantly for $\mathrm{Re}_b > 10$, particularly at small h.
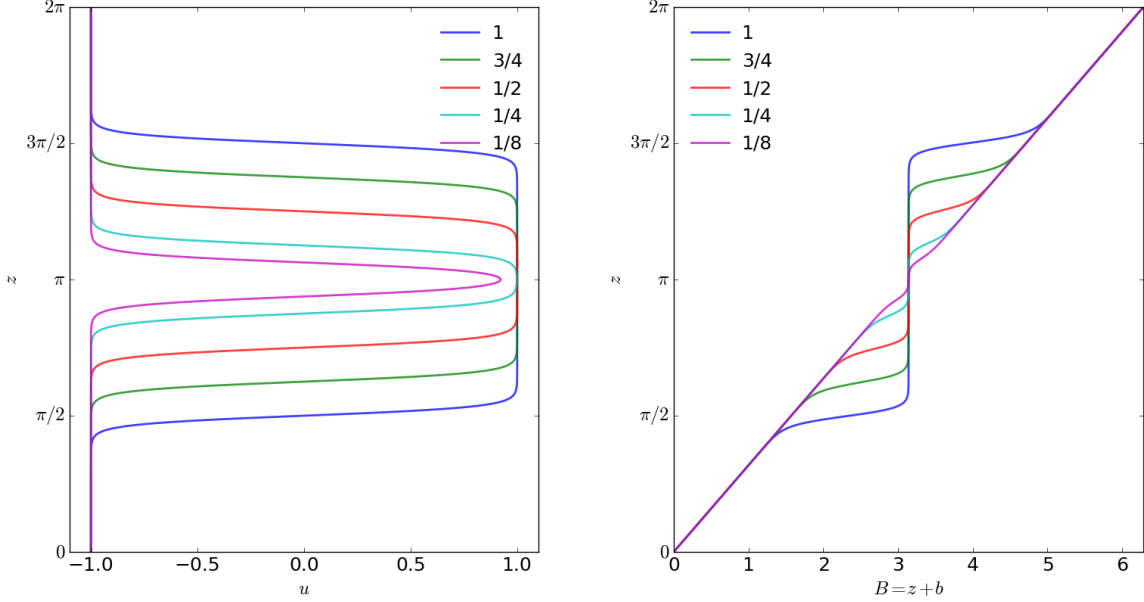
Figure 2: The initial condition for the toy decaying problem. We use various values of h, the distance between the two shear layers. (Left) horizontal velocity and (right) buoyancy.

These modes are stratified shear instablities. Figure 4 depicts the wavestructure for the most unstable modes in two cases: $h = 1$ and $h = 8$. The structure of the vertical velocity clearly show the classic "tilt against the shear". Also clearly depicted is the fact that with $h = 1$ the shear layers are independent whereas with $h = 1/8$ they are coupled. These modes are not classic Kelvin-Helmholtz instablities, e.g., Drazin & Reid [5]. In particular, the vorticity structure of these instabilities are composed of opposite sign votices with a phase shift.

3.2 Initial value problems

We now consider simulations of initial value problems. In particular, we discuss the structure of different solutions with varying h and Re_b. All simulations are initialized with the initial conditions (Figure 2). The perturbations are initialized with a small seed (10^{-6}) random field.

Figure 5 shows the time series for the evolution of the kinetic energy (KE) and potential energy (PE) of both slow/long fields and perturbations for an experiment with $\mathrm{Re}_b = 10$ and $h = 1$. With these parameters, the mean flow is signigicatlly damped by viscosity and diffusivity. Nevertheless, even at low Re_b, there is an interesting interaction between the mean (slow/long) fields and the perturbations. Once the pertubartions pick the right phase, they grow exponentially, with a rate consistent with the prediction of the linear stability analysis (see dashed green line in figure 5). The perturbations peak at about $t = 5$, and rapidly decay. This rapid decay is not accounted for by the viscous terms. Indeed, the perturbations accelerate the flow in the initial phase of their decay (see snapshots of slow velocity in the bottom panel of figure 5). For times larger than about 10, the perturbations have decayed significantly, so that the mean flow diffusively
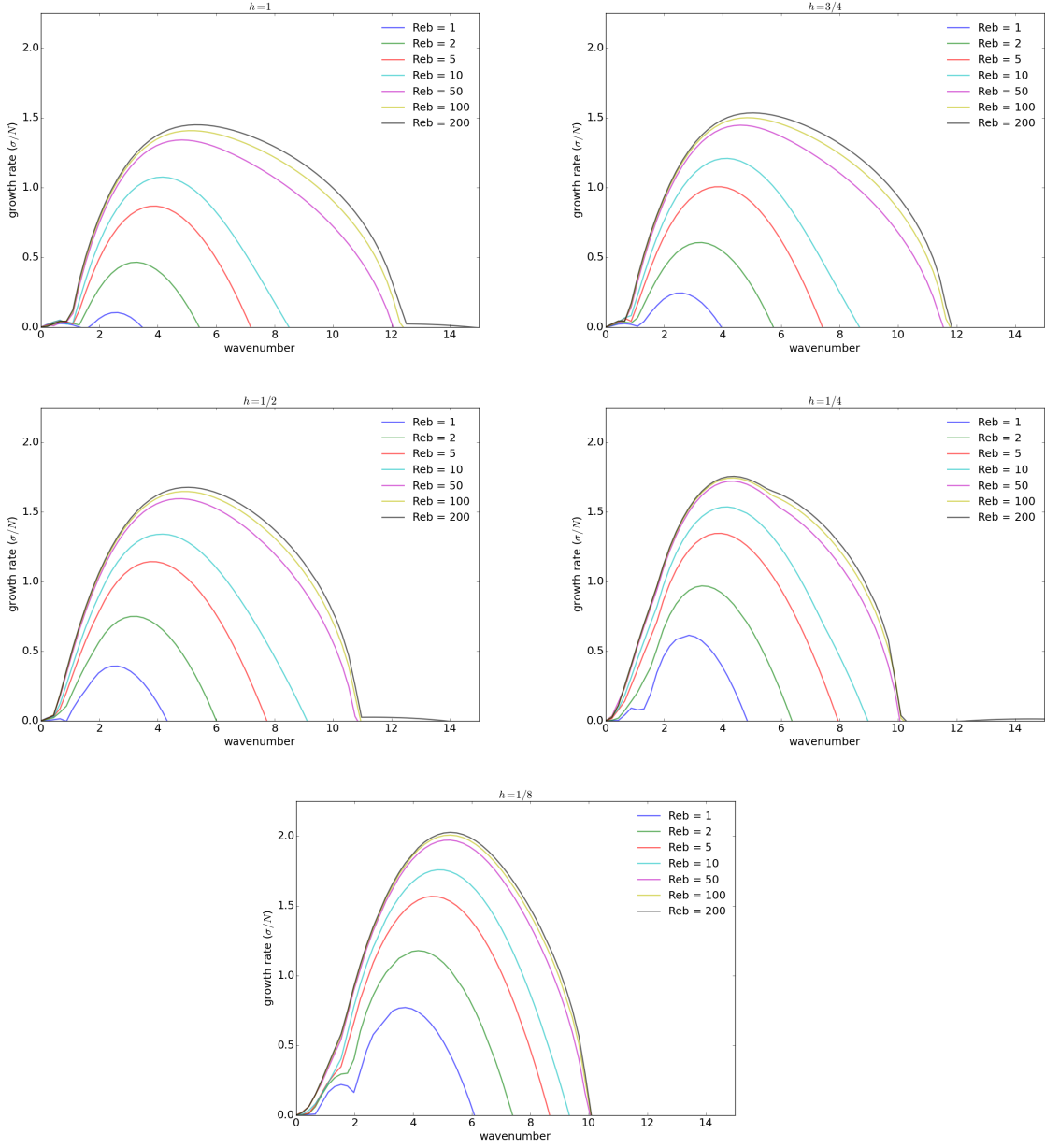
Figure 3: Growth rates for linear unstable modes for initial conditions with $h = 1$, $h = 3/4$, $h = 1/2$, $h = 1/4$, and $h = 1/8$.

tends towards a state of rest with linear stratification.

Increasing Re_b changed qualitatively and quantitatively that picture. For instance, figure 11 shows the time series of the different components of energy for an experiment with $\text{Re}_b = 200$ and $h = 1$. As in the $\text{Re}_b = 10$ case, the perturbations growth eponentially after picking up the right phase, and the growth rate is consistent with the predictions for the most unstable mode. However, at about $t = 4$, the perturbations

8
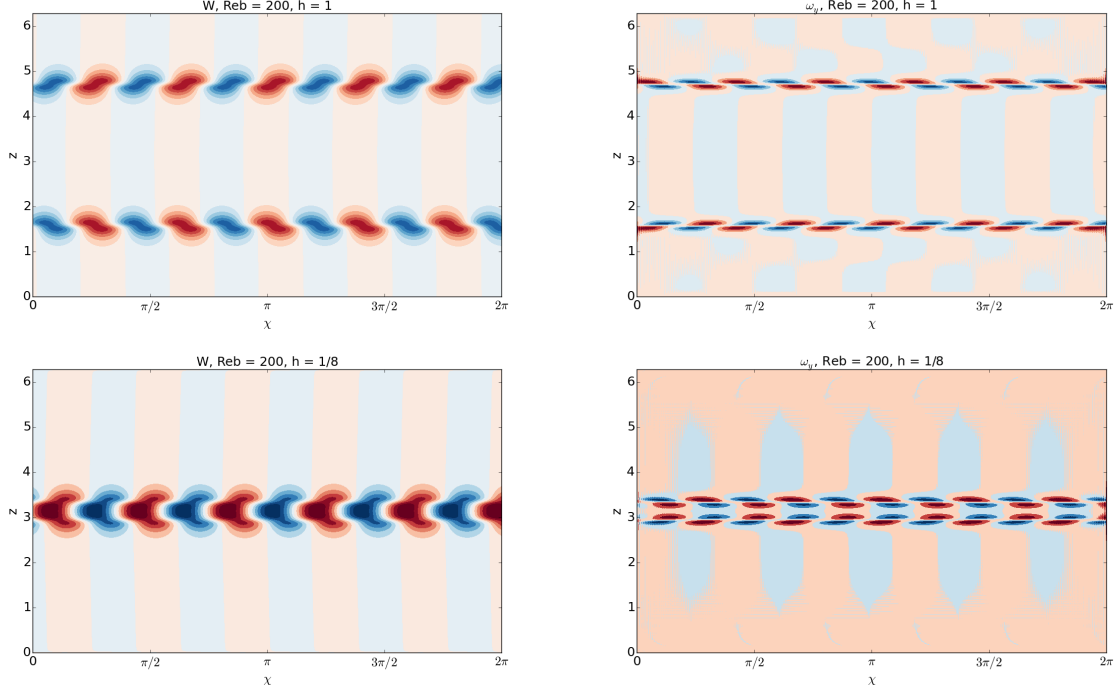
Figure 4: The wavestructure of the unstable modes for $h = 1$ (top) and $h = 1/8$ (bottom): (left) vertical velocity and (right) horizontal vorticity.

saturate. Because there are no non-linearities in the equatins for the perturbations, this saturation is due to a change in the slow horizontal velocity and buoyancy profiles. The perturbations then plateau for about 5 time units before they start decay. The initial decay is relatively fast, and it is not accounted for by viscosity. Indeed, as the perturbations decay, they accelerate the slow flow (see lower panel of figure 11), significantly changing its shape. At about $t = 60$, the perturbations start decaying very slowly, consistent with the visous and diffusive rates. The slow buoyancy profile is also significantly changed. In particular, regions initially strongly stratified are mixed up, and part of the region initially nearly mixed are restratified.

Reducing h allows for the two shear layers to interact. In particular, with $h = 1/8$, the initial condition is essentially a jet localized in the middle of the domain. With relatively large Re_b, the evolution of the energy is similar to the cases . The perturbations grow exponentially, and then quickly saturate. The decay of the perturbations also occur in two stages, first a relatively fast decay, followed by a slow viscous decay. However, in this case the mean flow is not accelerated during the decay of the perturbations. That is, for this particular case, the buoyancy flux and the Reynolds stress are sign-definite.

3.3 Bulk properties

To characterize the solutions of this model problem in parameter space, we calculate some diagnostic bulk propoerties. In particular, the energy partition of the perturbations is
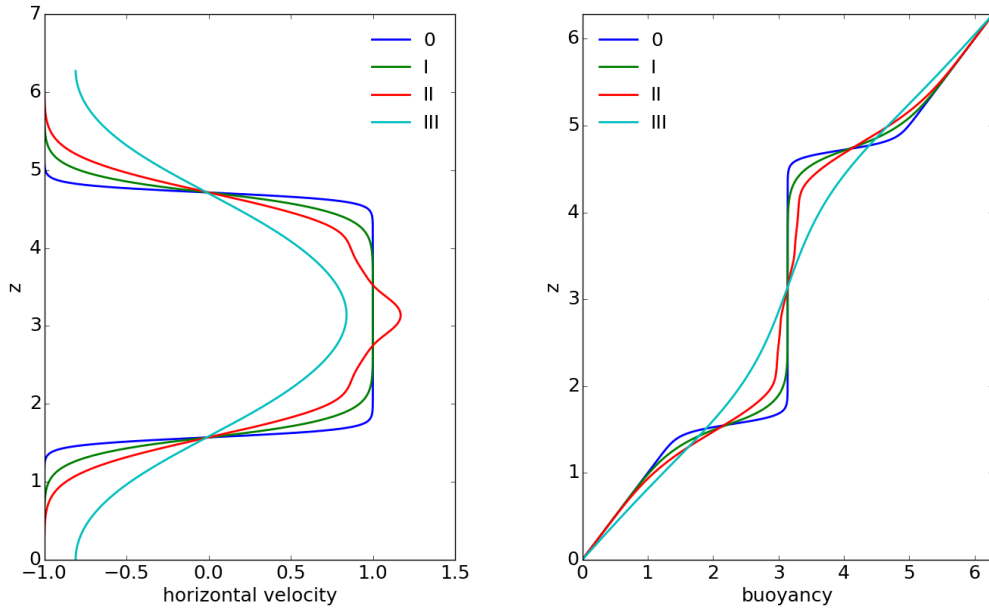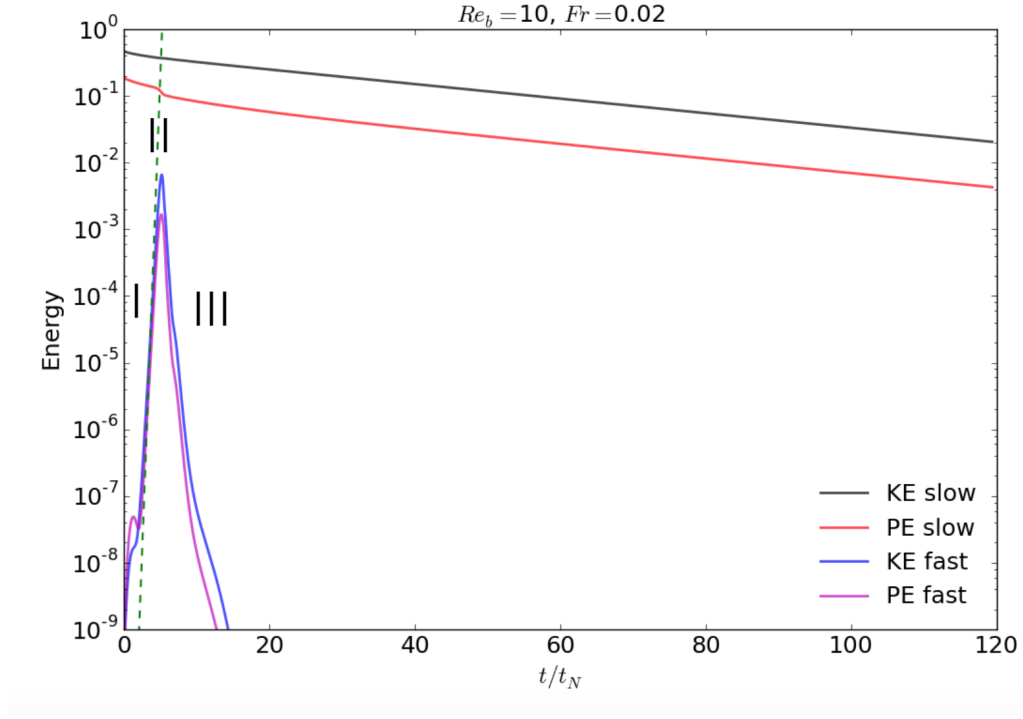
Figure 5: Solution to the IVP with $Re_b = 10$ and $h = 1$. The upper panel show the time series for different components of energy. The bottom panels depict the evolution of the slow flow at different stages (marked in the energy plot). The green dashed line depicts the linear growth for the most unstable mode.
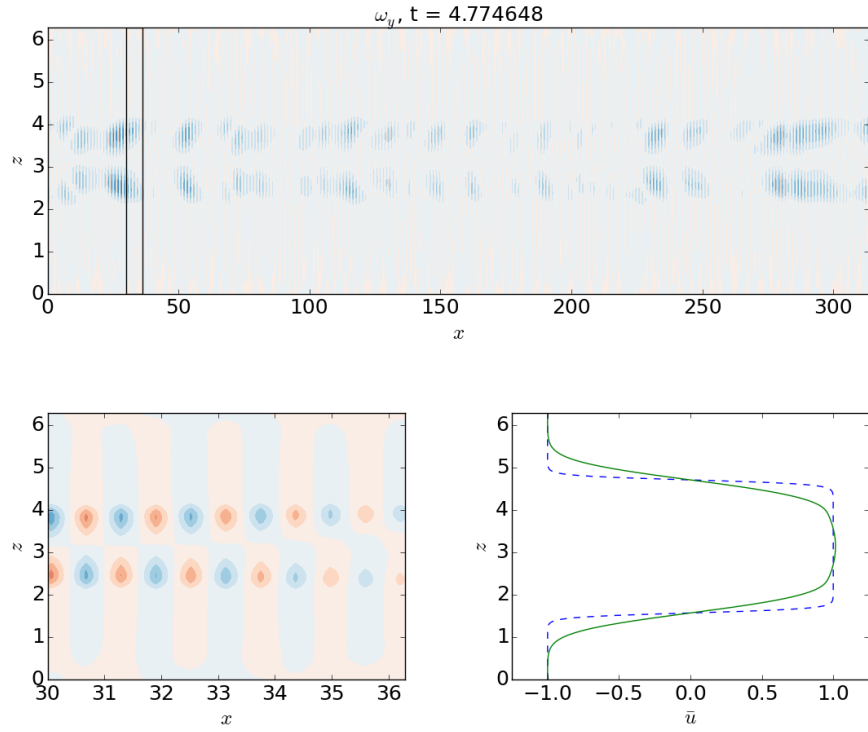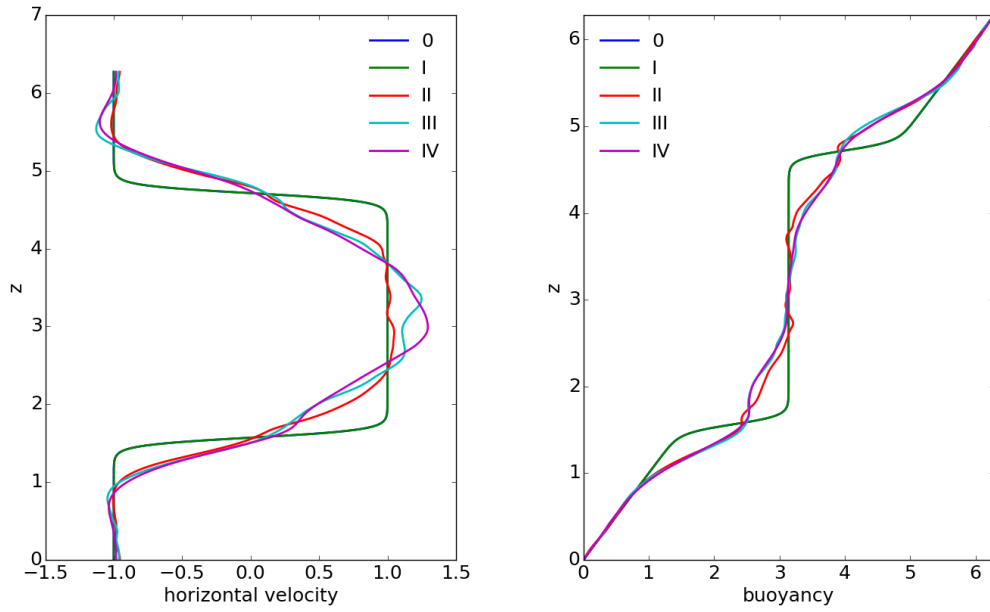
Figure 6: Snapshot of the structure of the solution to the IVP with $\mathrm{Re}_b = 10$ and $h = 1$. The upper panel shows the horizontal vorticity field. The lower left panel is a zoom-in of the upper panel in the region marked by the black square. The lower right panel shows the snapshot of the slow horizontal velocity (green) together with the initial condition.
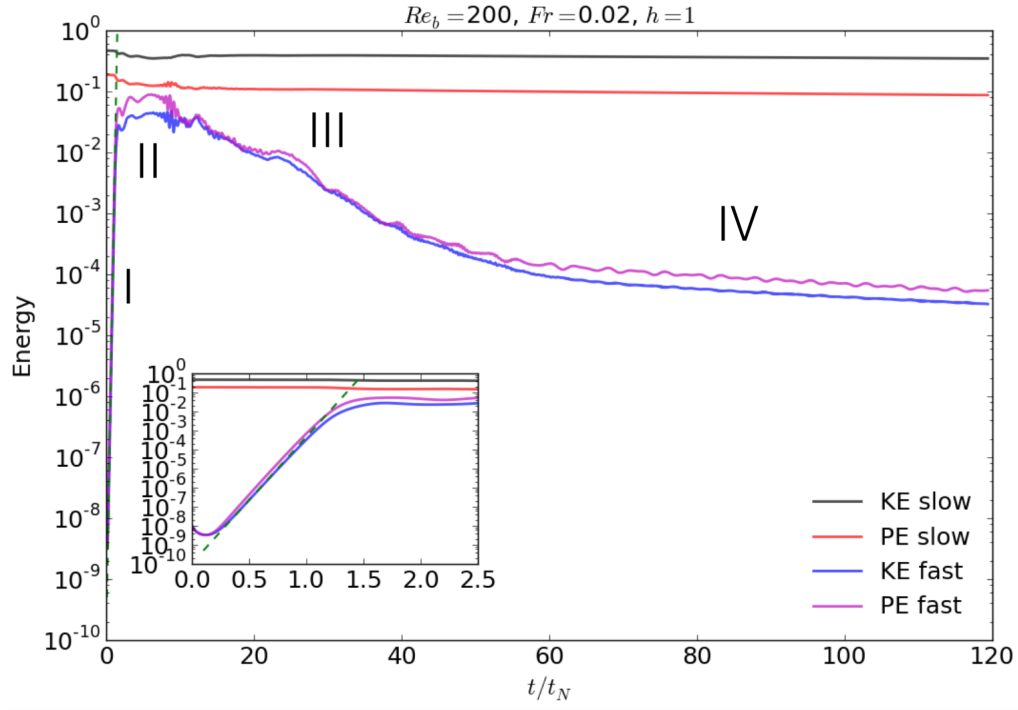
Figure 7: Solution to the IVP with $\mathrm{Re}_b = 200$ and $h = 1$. The upper panel show the time series for different components of energy. The bottom panels depict the evolution of the slow flow at different stages (marked in the energy plot). The green dashed line depicts the linear growth for the most unstable mode.
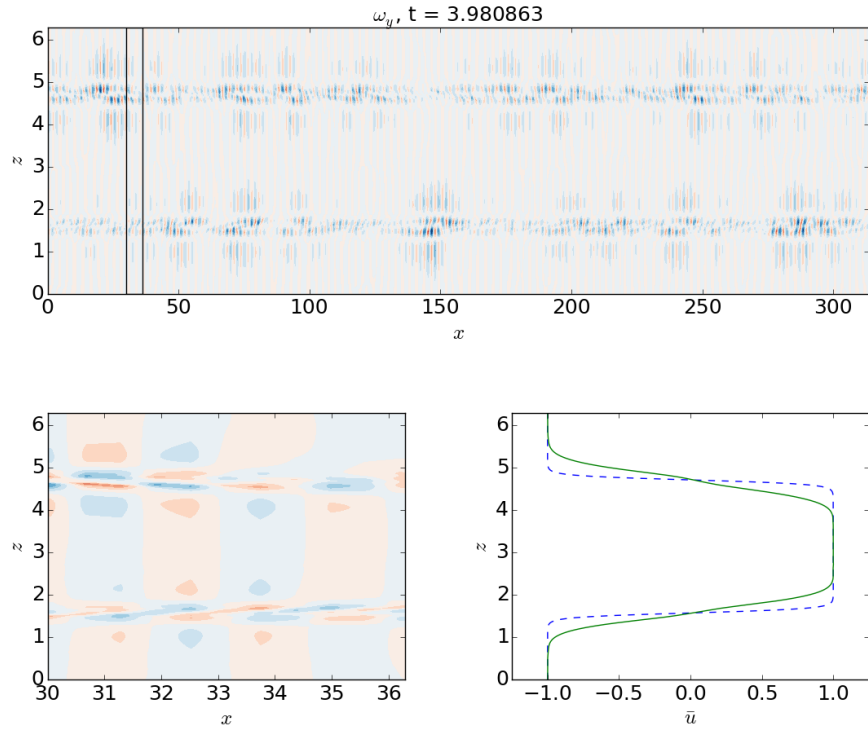
12

Figure 8: Snapshot of the structure of the solution to the IVP with $\mathrm{Re}_b = 200$ and $h = 1$. The upper panel shows the horizontal vorticity field. The lower left panel is a zoom-in of the upper panel in the region marked by the black square. The lower right panel shows the snapshot of the slow horizontal velocity (green) together with the initial condition.
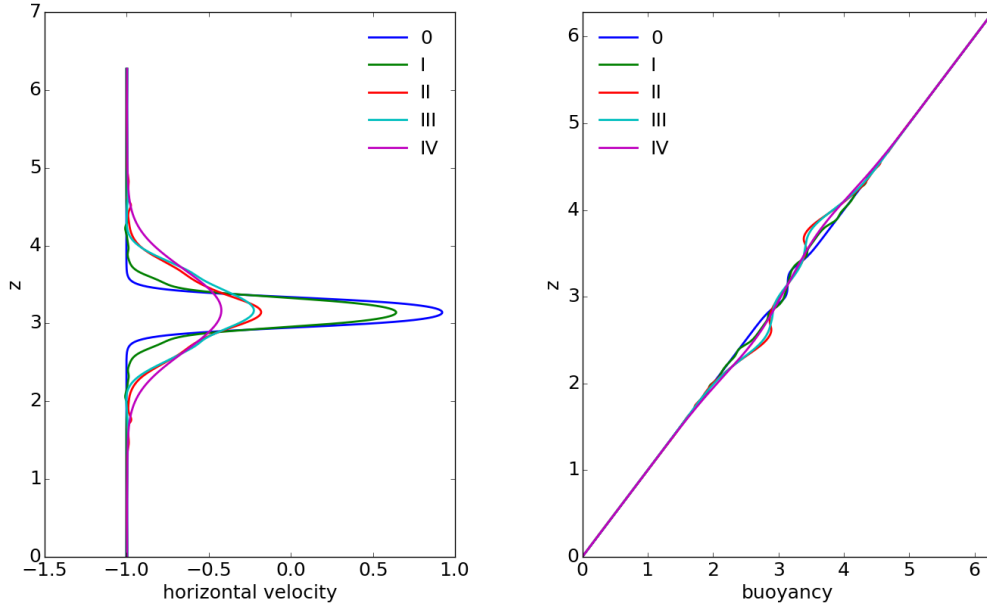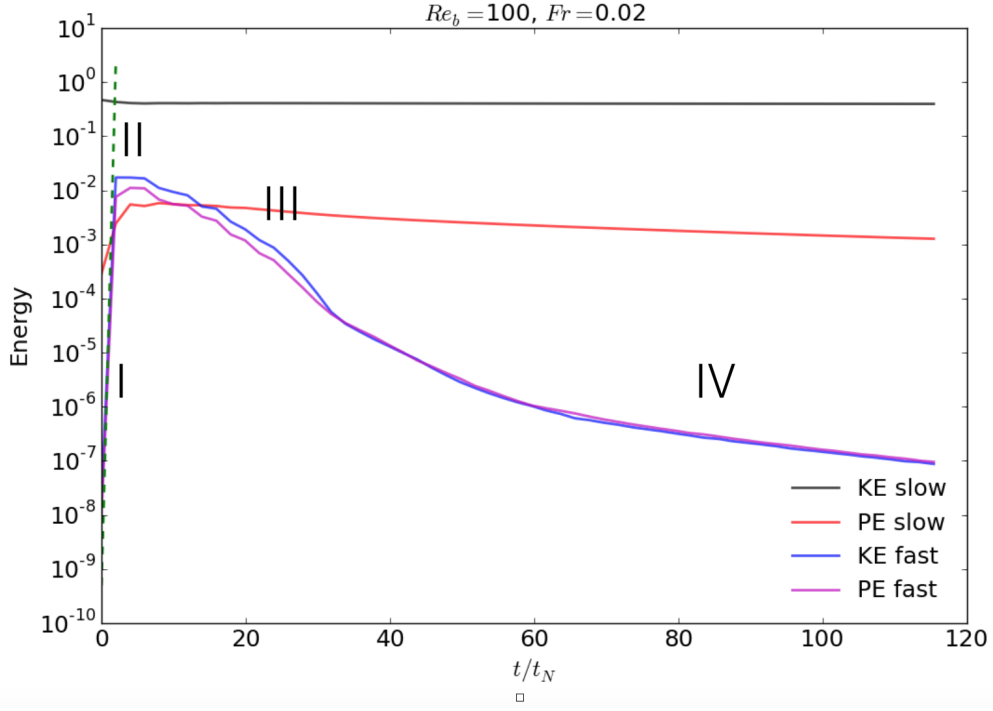
13

Figure 9: Solution to the IVP with $\mathrm{Re}_b = 100$ and $h = 1_8$. The upper panel show the time series for different components of energy. The bottom panels depict the evolution of the slow flow at different stages (marked in the energy plot). The green dashed line depicts the linear growth for the most unstable mode.
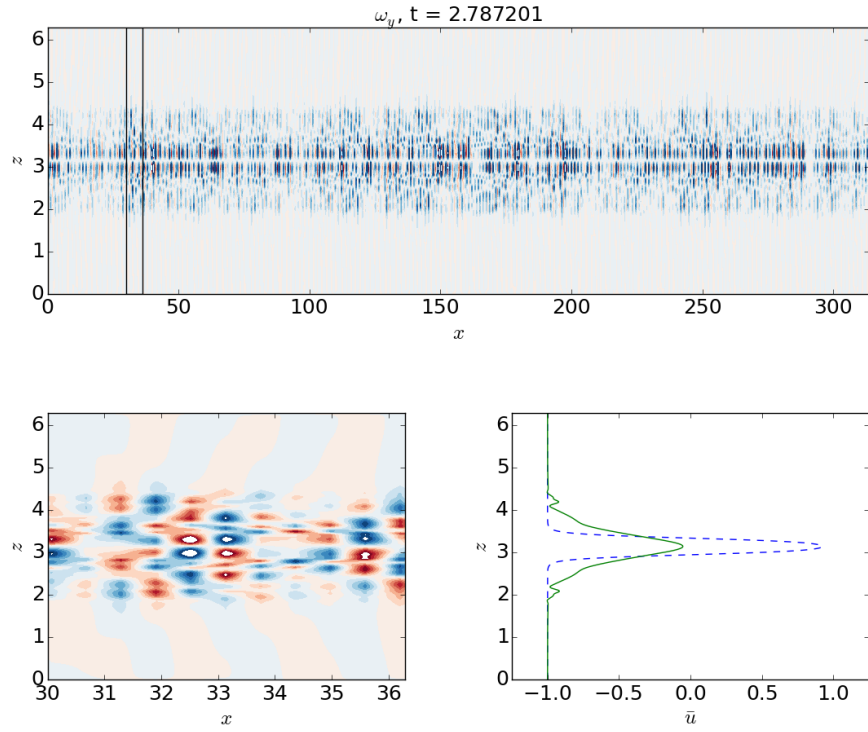
14

Figure 10: Snapshot of the structure of the solution to the IVP with $\mathrm{Re}_b = 100$ and $h = 1/8$. The upper panel shows the horizontal vorticity field. The lower left panel is a zoom-in of the upper panel in the region marked by the black square. The lower right panel shows the snapshot of the slow horizontal velocity (green) together with the initial condition.

$$\gamma \stackrel{\text{def}}{=} \frac{PE_{fast}}{PE_{fast} + KE_{fast}} \, . \tag{45}$$

This particular bulk property is of interest because it is a proxy of mixing efficiency. Because we are dealing with unforced problem, this property is calculated when the perturbations peak or saturate. Figure 11 shows the distribution of γ in the $h - \text{Re}_b$ space. Typically, γ increases with h, with maximum values of 0.7 for $h = 1$ (and $\text{Re}_b \geq 50$); γ is about 0.35 for $h = 1/8$. More over, it is quite surprising that for $\text{Re}_b \geq 50$, γ is nearly independent of Re_b. There is no simple scaling arguments that collapse this data into a single curve. That is, γ is not a simple function of h or the initial potential energy.

We also calculate the gain of the perturbations

$$G \stackrel{\text{def}}{=} 2 \times 10^6 \times (KE_{fast} + PE_{fast}) \, , \tag{46}$$

where we remind the reader that 10^{-6} is the magnitude of the initial random seed. First, we note that G is relatively large ($> 10^7$) across the parameter space (Figure 11). The pattern of G, however, has much more structure than the pattern of γ. As expected, the gain typically increases with Re_b. Also G is minumum for $h = 1/8$ likely because the initial potential energy is much smaller than with larger h. G peaks for $1/2 \leq h \leq 3/4$.
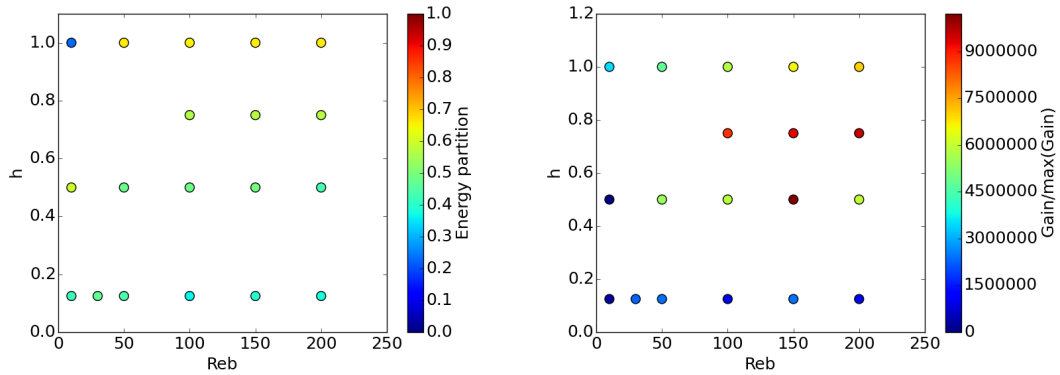

Figure 11: Bulk properties as a function of Re_b and h. (Left) Energy partition and (right) energy gain.

4   Final remarks

In this study we have taken advantage of the strong anisotropy driven by strong stratification to simplify the modeling of stratified turbulent flows. In particular, the asymptotics lead to the hydrostratic primitive equations of oceanography for the slow fields coupled by the vertical divergence of the Reynolds stress and buoyancy flux to a quasilinear system for the perturbations. Because the system is quasi-linear for the perturbations, there is no closure problem; the system is closed.

Using a simple toy problem, we have demonstrated the properties and utility of this reduced system. This example shows that the coupled system displays interesting dynamics with $\mathcal{O}(1)$ feedbacks between mean and perturbations. We emphasize that

the Reynolds stresses and buoyancy fluxes associated with the perturbations are not sign-definite in many regions of the parameter space.

Future work include introducing back variations in slow spatial coordinate, and therefore assessing the importance of vertical vorticity in the slow flow; comparisons with direct numerical simulations; and three-dimensional solutions. It is our hope that these equations would be used to study strongly stratified turbulent flows in regions of the parameter of geophysical relevance, which are currently unattainable through direct numerical simulations.

Acknowledgements

A   The self-similarity of strongly stratified flows

This appendix justifies the scaling choice $\text{Fr} \sim \alpha$, which implies that the vertical scale is $\mathcal{H} \sim \mathcal{U}/N$. Following [2] we consider the dimensional inviscid Boussinesq equations in the limit $\text{Fr} \to 0$

$$\partial_t \boldsymbol{u}_h + \boldsymbol{u}_h \cdot \boldsymbol{\nabla}_h \boldsymbol{u}_h + w\partial_z \boldsymbol{u}_h = -\boldsymbol{\nabla}_h \phi \,, \tag{47}$$

$$0 = -\partial_z \phi + b \,, \tag{48}$$

$$\boldsymbol{\nabla}_h \cdot \boldsymbol{u}_h + \partial_z w \,, \tag{49}$$

and

$$\partial_t b + \boldsymbol{u}_h \cdot \boldsymbol{\nabla}_h b + w\partial_z b = w \,, \tag{50}$$

Equations (47) through (50) are invariant under the transformations

$$N = N^*/A \,, \qquad z = Az* \,, \qquad w = A\,w^* \,, \qquad \text{and} \qquad b = b^*/A \,, \tag{51}$$

where A is a constant. Thus, for constant N, the solutions to (47) through (50) can be determined from the solutions from the same equations with $N^* = 1$. With $A = 1/N$, we have

$$\boldsymbol{u}_h = \boldsymbol{u}_h^*(x, y, zN, t) \,,$$

$$w = \frac{1}{N}w^*(x, y, zN, t) \,,$$

$$b = Nb^*(x, y, zN, t) \,. \tag{52}$$

Note that the vertical length scale is inversely proportional to the buoyancy frequency; as the stratification increases the vertical scale decreases $\mathcal{H} \propto 1/N$. Thus, on dimensional grounds, we have $\mathcal{H} \sim \mathcal{U}/N$. This self similarity implies that $\text{Fr} \sim \alpha$, and therefore as $\text{Fr} \to 0$, the aspect ratio adjusts so that the ratio Fr/α remains $\mathcal{O}(1)$. This has profound consequences for the dynamics because the system does not become two-dimensional as $\text{Fr} \to 0$.

B   The Taylor-Goldstein equation

Consider the inviscid two-dimensional (x, z) version of equation (37).

$$(\partial_\tau + \bar{u}\partial_\chi)\left[(\partial_\tau + \bar{u}\partial_\chi)\left(\partial_\chi^2 + \partial_z^2\right) - \partial_z^2\bar{u}\partial_\chi\right]w' + (\partial_z\bar{b} + 1)\partial_\chi^2 w' = 0 \,. \tag{53}$$

Now, we assume wave-like solutions $w' = \hat{w}(z)\mathrm{e}^{\mathrm{i}k(x-c\tau)}$, to obtain

$$(\bar{u} - c)^2\left(\hat{w}_{zz} - k^2\hat{w}\right) + \left[\underbrace{(\bar{b}_z + 1)}_{\equiv N^2(z)} - (\bar{u} - c)\,\bar{u}_{zz}\right]\hat{w} = 0 \,, \tag{54}$$

which is the celebrated Taylor-Goldstein equation. In a bounded vertical domain of length 2π, we assume no-normal flow at the boundaries, which reduces to

$$\hat{w} = 0 \,, \qquad z = 0,\, 2\pi \,. \tag{55}$$

The Taylor-Goldstein equation has been significantly analyzed. Among the most important results, the sufficient condition for stability due to John Miles and Lou Howard is that the gradient Richardson's number be greater than a quarter:

$$\text{Ri} \overset{\text{def}}{=} \frac{N^2(z)}{\bar{u}_z^2} > \frac{1}{4} \,. \tag{56}$$

Also, again due to Lou Howard, the unstable phase speed $c_r \overset{\text{def}}{=} \text{Re}\{c\}$ is bounded by $\bar{u}_{min} < c_r < \bar{u}_{max}$, and $c_i \overset{\text{def}}{=} \text{Im}\{c\}$ is bounded by

$$c_i^2 \leq \left[\tfrac{1}{2}\left(\bar{u}_{max} - \bar{u}_{min}\right)\right]^2 - \left[c_r - \tfrac{1}{2}\left(\bar{u}_{max} + \bar{u}_{min}\right)\right]^2 . \tag{57}$$

An upper bound on the growth rate is

$$k\,c_i \leq \frac{k}{2}\left(\bar{u}_{max} - \bar{u}_{min}\right) . \tag{58}$$

C   Conservation of energy

We form an equation for the kinetic energy of the slow/large flow by dotting the (25) and adding to $\bar{w}$ times (28) to obtain

Slow flow

$$\partial_t \tfrac{1}{2}|\bar{\boldsymbol{u}}_h|^2 = \bar{w}\bar{b} + \overline{w'\boldsymbol{u}_h'}\cdot\partial_z\bar{\boldsymbol{u}}_h + \boldsymbol{\nabla}_h^{\boldsymbol{x}}\cdot\boldsymbol{T^x} + \partial_z\,T^z - \frac{1}{\text{Re}_b}\,|\partial_z\bar{\boldsymbol{u}}_h|^2 , \tag{59}$$

where

$$\boldsymbol{T^x} = -\bar{\boldsymbol{u}}_h\left(\bar{p} + \tfrac{1}{2}|\bar{\boldsymbol{u}}_h|^2\right) , \tag{60}$$

$$T^z = \frac{1}{\text{Re}_b}\partial_z\tfrac{1}{2}|\bar{\boldsymbol{u}}_h|^2 + \bar{\boldsymbol{u}}_h\cdot\overline{w'\boldsymbol{u}_h'} - \bar{w}p . \tag{61}$$

and we used the continuity equation (27). Similarly, an equation for the potential energy density is formed by multiplying (28) by $\bar{b}$

$$\partial_t \tfrac{1}{2}\bar{b}^2 = -\bar{w}\bar{b} + \overline{w'b'}\partial_z\bar{b} + \boldsymbol{\nabla}_h^{\boldsymbol{x}}\cdot\boldsymbol{B^x} + \partial_z B^z - \frac{1}{\text{Re}\,\text{Pr}}\left(\partial_z b\right)^2 , \tag{62}$$

where

$$\boldsymbol{B^x} = -\bar{\boldsymbol{u}}_h\tfrac{1}{2}\bar{b}^2 , \tag{63}$$

and

$$B^z = \frac{1}{\text{Re}_b\,\text{Pr}}\partial_z\tfrac{1}{2}b^2 + -\bar{w}\tfrac{1}{2}\bar{b}^2 - \bar{b}\,\overline{w'b'} . \tag{64}$$

The equation for the slow/large scale total energy is then

$$\partial_t \tfrac{1}{2}\left(|\bar{\boldsymbol{u}}_h|^2 + \bar{b}^2\right) = \overline{w'\boldsymbol{u}_h'}\cdot\partial_z\bar{\boldsymbol{u}}_h + \overline{w'b'}\partial_z\bar{b} + \boldsymbol{\nabla}_h^{\boldsymbol{x}}\cdot(\boldsymbol{T^x} + \boldsymbol{B^x}) + \partial_z\left(T^z + B^z\right) . \tag{65}$$

Fast flow

To obtain an equation for the energy density of the fast flow, we dot (33) with $\boldsymbol{u}_h'$, add to w' times (34), and average over the fast time to obtain

$$\text{Fr}\,\partial_t\tfrac{1}{2}\left(\overline{\boldsymbol{u}_h'^2} + \overline{w'^2}\right) = \overline{w'b'} - \overline{\boldsymbol{u}_h'w'}\partial_z\bar{\boldsymbol{u}}_h' + \boldsymbol{\nabla}_h^{\boldsymbol{x}}\cdot\boldsymbol{T_2^x} + \partial_z\,T_2^z - \frac{\text{Fr}}{\text{Re}_b}\left(\text{Fr}^2\overline{|\boldsymbol{\nabla}_h^{\boldsymbol{x}}\boldsymbol{u}_h'|^2} + \overline{|\partial_z\boldsymbol{u}_h'|^2}\right) , \tag{66}$$

where

$$\boldsymbol{T_2^x} = -\text{Fr}\bar{\boldsymbol{u}}_h\left(p' + \tfrac{1}{2}\overline{|\boldsymbol{u}_h'|}^2 + \tfrac{1}{2}\overline{w'^2}\right) + \frac{\text{Fr}^3}{\text{Re}_b}\boldsymbol{\nabla}_h^{\boldsymbol{x}}\tfrac{1}{2}\overline{|\boldsymbol{u}_h'|^2} , \tag{67}$$

$$T_2^z = \bar{\boldsymbol{u}}_h\cdot\overline{w'\boldsymbol{u}_h'} - \bar{w}p + \frac{\text{Fr}}{\text{Re}_b}\partial_z\tfrac{1}{2}\overline{|\boldsymbol{u}_h'|^2} . \tag{68}$$

19

Similarly, we obtain an equation for the potential energy density of the perturbation

$$\text{Fr}\,\partial_t \tfrac{1}{2}\overline{b'^2} = -\overline{w'b'} - \overline{w'b'}\partial_z\bar{b} + \boldsymbol{\nabla}_h^{\boldsymbol{x}} \cdot \boldsymbol{B}_2 + \partial_z B_z - \frac{1}{\text{Re}_b\text{Fr}}\left(\text{Fr}^2\overline{|\boldsymbol{\nabla}_h^{\boldsymbol{x}} b'|^2} + (\partial_z b')^2\right). \quad (69)$$

where

$$\boldsymbol{B}_2^{\boldsymbol{x}} = -\text{Fr}\tfrac{1}{2}\boldsymbol{\nabla}_h^{\boldsymbol{x}} \cdot \bar{\boldsymbol{u}}_h\overline{b'^2} + \frac{\text{Fr}^3}{\text{Re}_b\,\text{Pr}}\boldsymbol{\nabla}_h^{\boldsymbol{x}}\tfrac{1}{2}\overline{b'^2}, \quad (70)$$

$$B_2^z = \frac{\text{Fr}}{\text{Re}_b\,\text{Pr}}\partial_z\overline{b'^2}. \quad (71)$$

The equation for the total energy for the leading order perturbations is

$$\text{Fr}\,\partial_t \tfrac{1}{2}\left(\overline{|\boldsymbol{u}_h'|^2} + \overline{w'^2} + \overline{b'^2}\right) = -\overline{w'\boldsymbol{u}_h'}\cdot\partial_z\bar{\boldsymbol{u}}_h - \overline{w'b'}\partial_z\bar{b} + \boldsymbol{\nabla}_h^{\boldsymbol{x}}\cdot(\boldsymbol{T}_2^{\boldsymbol{x}} + \boldsymbol{B}_2^{\boldsymbol{x}}) + \partial_z\left(T_2^z + B_2^z\right). \quad (72)$$

D Sensitivity of numerical solutions to time averaging

Formally, the averaging over the small scales is defined over time and space (23). For computational convenience, however, it is convenient to march coupled system of PDEs without with a single time-scale without time-averaging. To test the sensitivity of the evolution to the system to time-averaging, we perform two numerical simulations with the same parameters ($Fr = 0.1$, $Re_b = 80$, $k_0 = 4.5$, $m_0 = 10$). Time-averaging the small/fast flow over $1/Fr$ has insignificant effect on the initial evolution of the slow flow (figure 12). The secondary stage stage of evolution of the flow has quantitative differences, but overall no dramatic qualitative differences. We therefore conclude that, for this set of parameters, not averaging on time is not qualitatively misleading. It is not obvious whether such results hold at smaller Froude numbers, but we nevertheless make this assumption for computational feasibility.

References

[1] P. Bartello and S. Tobias, *Sensitivity of stratified turbulence to the buoyancy reynolds number*, Journal of Fluid Mechanics, 725 (2013), pp. 1–22.

[2] P. Billant and J.-M. Chomaz, *Self-similarity of strongly stratified inviscid flows*, Physics of Fluids, 13 (2001), pp. 1645–1651.

[3] G. Brethouwer, P. Billant, E. Lindborg, and J.-M. Chomaz, *Scaling analysis and simulation of strongly stratified turbulent flows*, Journal of Fluid Mechanics, 585 (2007), pp. 343–368.

[4] J. Callies, R. Ferrari, and O. Bühler, *Transition from geostrophic turbulence to inertia–gravity waves in the atmospheric energy spectrum*, Proceedings of the National Academy of Sciences, 111 (2014), pp. 17033–17038.

[5] P. G. Drazin and W. H. Reid, *Hydrodynamic stability*, Cambridge University Press, 2004.

[6] K. Julien and E. Knobloch, *Reduced models for fluid flows with strong constraints*, Journal of Mathematical physics, 48 (2007), p. 065405.

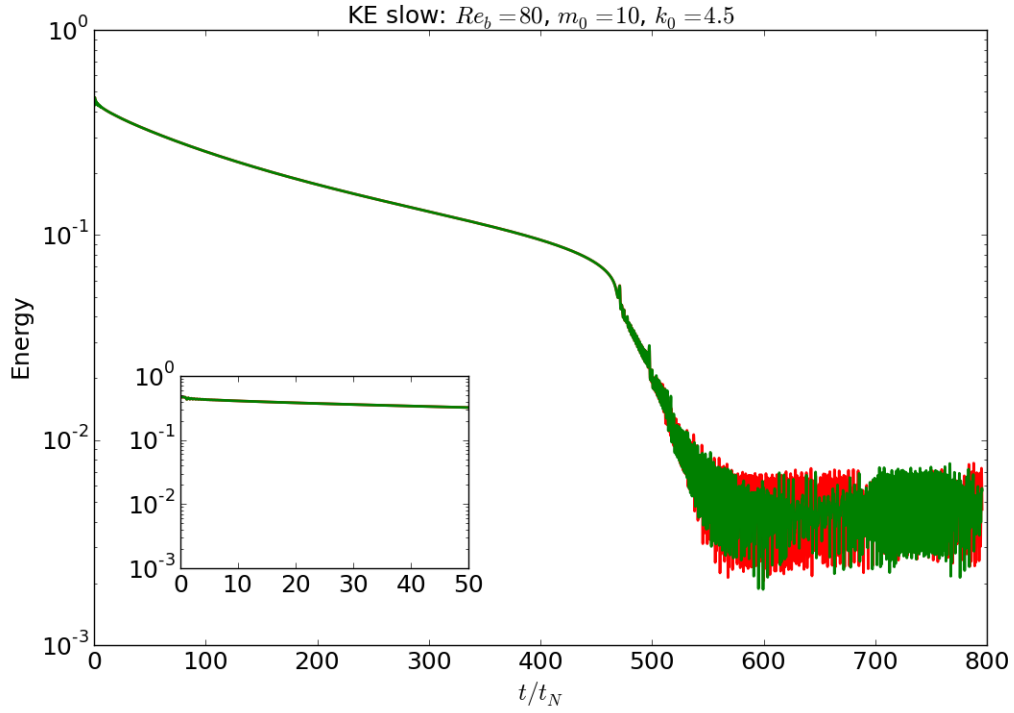[7] J. Riley and E. Lindborg, *Recent progress in stratified turbulence*, (2010).

Figure 12: Kinetic energy of the slow flow for experiments with (red) and without (green) averaging. The results are very similar in the initial stages, but differ quantitatively in the secondary, oscillatory state.

[8] M. Sprague, K. Julien, E. Knobloch, and J. Werne, *Numerical simulation of an asymptotically reduced system for rotationally constrained convection*, Journal of Fluid Mechanics, 551 (2006), pp. 141–174.

[9] G. K. Vallis, *Atmospheric and oceanic fluid dynamics: fundamentals and large-scale circulation*, Cambridge University Press, 2006.